INVITED PAPER

Adaptive Wireless Power Transfer and Backscatter Communication for Perpetual Operation of Wireless Brain–Computer Interfaces

This article describes efforts in eliminating tethers in brain–computer interfaces (BCIs) used in fundamental neurophysiology research.

By GREGORY E. MOORE, *Member IEEE*, JAMES D. ROSENTHAL, *Member IEEE*, JOSHUA R. SMITH, *Fellow IEEE*, AND MATTHEW S. REYNOLDS, *Senior Member IEEE*

ABSTRACT | Brain–computer interfaces (BCIs) are neural prosthetics that enable closed-loop electrophysiology procedures. These devices are currently used in fundamental neurophysiology research, and they are moving toward clinical viability for neural rehabilitation. State-of-the-art BCI experiments have often been performed using tethered (wired) setups in controlled laboratory settings. Wired tethers simplify power and data interfaces but restrict the duration and types of experiments that are possible, particularly for the study of sensorimotor pathways in freely behaving animals. To eliminate tethers, there is significant ongoing research to develop fully wireless BCIs having wireless uplink of broadband neural recordings and wireless recharging for long-duration deployment, but significant challenges persist. BCIs must deliver complex functionality while complying with tightly coupled constraints in size, weight, power, noise, and biocompatibility. In this article, we provide an overview of recent progress in wireless BCIs and a detailed presentation of two emerging technologies that are advancing the state of the art: ultralow-power wireless backscatter communication and adaptive inductive resonant (AIR) wireless power transfer (WPT).

KEYWORDS | Backscatter communication; biomedical devices; neural recording; wireless power transfer (WPT).

Manuscript received June 29, 2021; revised October 31, 2021 and November 13, 2021; accepted November 14, 2021. Date of publication December 10, 2021; date of current version January 6, 2022. This work was supported in part by the National Science Foundation Graduate Research Fellowship under Grant DGE-1762114, in part by the National Science Foundation Award under Grant EEC-1028725, in part by the National Science Foundation under Award EEC-1028725, in part by the Center for Neurotechnology, in part by the University of Washington Institute for Neuroengineering, and in part by the Washington National Primate Research Center. The work of James D. Rosenthal was supported by the National Science Foundation under Grant DGE-1762114. *(Gregory E. Moore, James D. Rosenthal, Joshua R. Smith, and Matthew S. Reynolds contributed equally to this work.) (Corresponding authors: Joshua R. Smith; Matthew S. Reynolds.)*

This work involved human subjects or animals in its research. Approval of all ethical and experimental procedures and protocols was granted by the University of Washington Institutional Animal Care and Use Committee.

Gregory E. Moore and **Matthew S. Reynolds** are with the Department of Electrical and Computer Engineering and the Center for Neurotechnology, University of Washington, Seattle, WA 98195 USA (e-mail: matt.reynolds@ece.uw.edu).

James D. Rosenthal is with the Swiss Federal Institute of Technology Lausanne (EPFL), 1015 Lausanne, Switzerland.

Joshua R. Smith is with the Department of Electrical and Computer Engineering, the Center for Neurotechnology, and the Allen School of Computer Science and Engineering, University of Washington, Seattle, WA 98195 USA (e-mail: jrs@cs.washington.edu).

Digital Object Identifier 10.1109/JPROC.2021.3130059

I. INTRODUCTION

The U.S. National Academy of Engineering (NAE) and the American Institute for Biological and Medical Engineering (AIBME) have identified the development of personalized, networked healthcare for neurological disorders to be particularly impactful for improving healthcare equality in the United States [1]. With many unknowns remaining about the healthy and pathological states of the nervous system, the NAE emphasized *reverse engineering the brain* as a key step toward developing translational

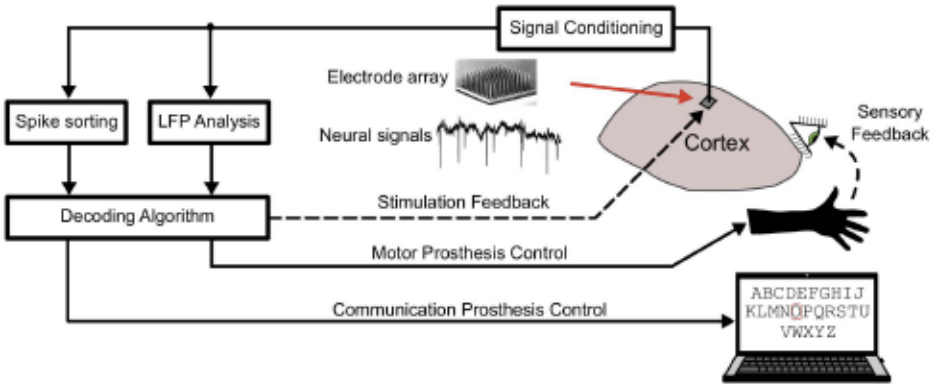

Fig. 1. *BCIs measure and process neural signals. A generalized architecture for neural prosthetics is shown (adapted from [2]).*

medical therapies. Aligned with this goal is the need to understand the underlying mechanisms of therapies, such as electrical stimulation in order to provide precise, personalized care.

Bidirectional brain–computer interfaces (BBCIs) are an emerging tool for investigating the electrophysiological mechanisms behind high-level sensory functions. These devices provide both recording of neural signals and feedback, e.g., via electrical stimulation, to manipulate those signals. A diagram of general BBCI architectures is shown in Fig. 1. Commonly targeted neural signals include local field potentials (LFPs) (10–300 Hz and 5 mV_{pp}) and action potentials (APs) (500–3000 Hz and 0.05–0.5 mV_{pp}), typically having a dc electrochemical offset of ± 50 mV and a noise floor of 0.014 mV_{rms} from 450 to 10 kHz [3]. To measure APs with sufficient temporal resolution for mammalian neurons, sampling rates greater than 20 kHz are desirable. Stimulation can be provided through several different modalities, including biphasic current pulses, or optogenetic and optoelectric [4] stimulation. Integrating recording and stimulation enables the fundamental study of how neural circuits can be rewired to repair or circumvent damaged neural pathways or deliver intracranial pattern reinforcement [5]. In the case of electrical stimulation, pulses delivered by the stimulating electrodes range from 5 V at 0.02 mA to 60 V at 10 mA via biphasic, possibly asymmetric, waveforms with pulse widths between 1 μs and 10 ms [6]. In addition to research applications, such bidirectional devices are increasingly studied for treating neurodegenerative disorders, such as Parkinson's disease [7] and amyotrophic lateral sclerosis (ALS) [8], spinal cord injury [9], and cognitive ailments, such as obsessive-compulsive disorder (OCD) [10].

Organization of This Article: This article is organized into six sections. Section II provides an overview of the state-of-the-art BBCIs. Section III further discusses the enabling technologies behind near-field resonant inductive coupling (NRIC) and backscatter communication. In Section IV, the specific implementations of NRIC and Neural Acquisition and Comms (NACs) using backscatter communication are explained in detail. Section V discusses topics for future research that could provide further improvements, while Section VI concludes this article.

II. INTRODUCTION TO THE BBCI STATE OF THE ART

A. Tethered Versus Wireless BBCIs

To achieve the recording and stimulation performance described above, existing BBCIs often rely on wired tethers to facilitate the transfer of power and data, as well as to enable an external computer to perform computationally intensive algorithms for closed-loop control, such as spike sorting and neural decoding. Significant advances continue to be made using tethered setups in human and animal subjects, including interpreting speech [8], control of a robotic arm [11], and high-rate typing [12]. When used with animal models, tethered experiments can provide reliable electronic interfaces and, in certain situations, can permit freely moving behavior within a constrained environment [13]. However, in larger animal models, such as nonhuman primates (NHPs), tethered experiments generally require significant physical constraints to protect the animals and the external equipment. The physical constraints pose several problems. Physical constraints are uncomfortable for animals, so the experimental durations are limited by the animal's attention span and tolerance. In research on motor tasks, physically limiting a subject's movement reduces the types of behaviors that can be analyzed. Furthermore, restricting motion has been shown to introduce unnatural correlations in the neural recordings [14]. There is also a risk of dangerous interactions between the animal and the researchers or technical staff whenever an animal must be removed from its cage to be placed within a constrained experimental setup. For example, researchers face an elevated risk of contracting the Simian herpes virus when handling or working with NHPs [15]. Finally, tethers provide a vector for infection of vulnerable tissues, and they can present electrical hazards if cable insulation is damaged or interconnects deteriorate.

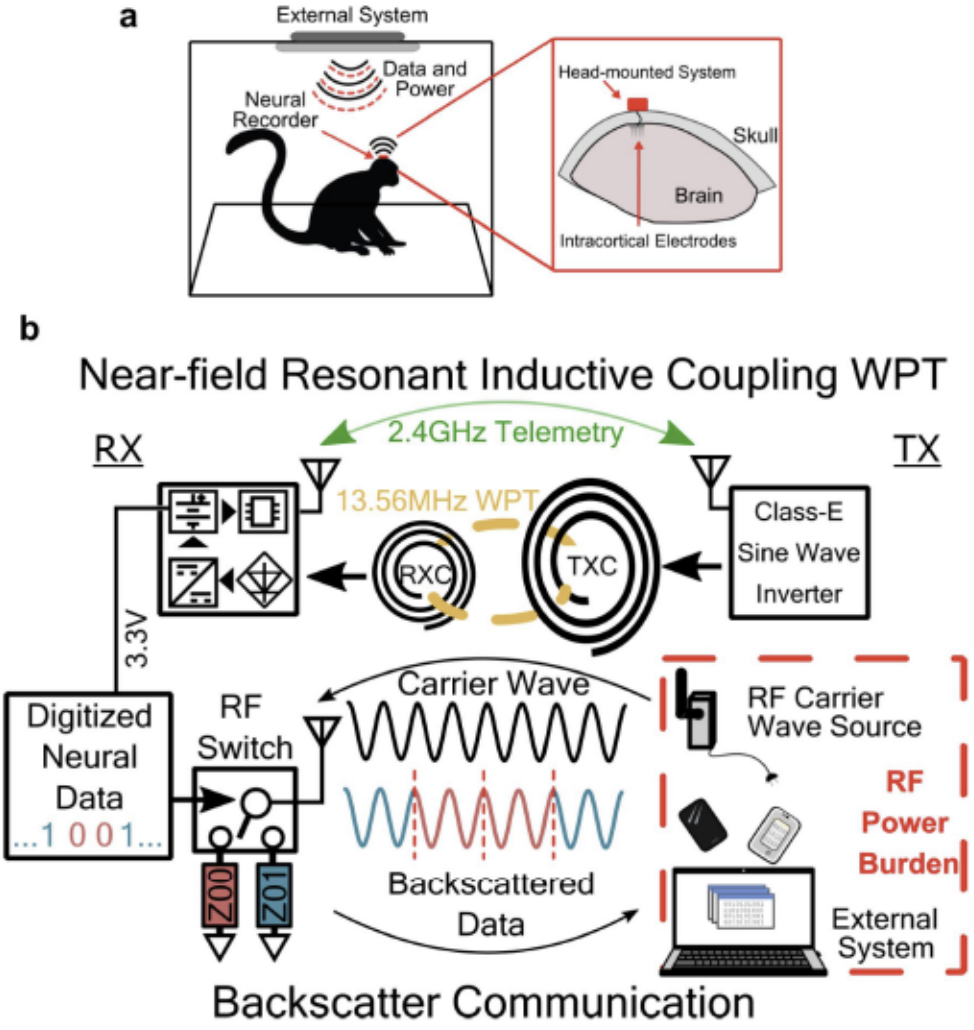

Fig. 2. *Overview of a perpetual wireless BCI leveraging NRIC WPT and backscatter communication. (a) Experimental setup for a wireless (untethered) BBCI system deployed in electrophysiological experiments on an NHP model. (b) Block diagram of the W-BBCI showing the wireless power and communication links.*

Fully wireless BBCIs (W-BBCIs), as shown in Fig. 2(a), seek to overcome the limitations of tethers, with many different architectures and form factors being explored. The design of the wireless power and communication aspects of W-BBCIs depend heavily on the intended recording and/or stimulation design which must accommodate size, weight, and power (SWaP) constraints. Because energy storage devices, such as batteries, trade off weight and volume for capacity, careful attention to power is perhaps the paramount design consideration. In addition, minimizing power dissipation on the BBCI device is important for minimizing thermal hazards to surrounding tissue. The power requirements of a BBCI system increase with channel count, sampling rate, signal resolution, and communication paradigm. At the same time, the communication link must be selected to accommodate the required data rate and transmission fidelity. To best accomplish these goals, many head-mounted external systems using commercial off-the-shelf (COTS) components [6], [16]–[19] and mm-scale implantable devices using custom application-specific integrated circuits (ASICs) complemented by COTS components [20]–[32] have been developed. As shown in Table 1, typical systems use variations on radio links ranging from 13.56 MHz to 7.9 GHz or, alternatively, variations on ultrasonic backscatter [33] in order to uplink recorded neural data to an external system for analysis and closed-loop applications.

The BBCI systems highlighted in Table 1 eliminate the tether by using combinations of rechargeable batteries (usually Li-ion), with a wireless power link for recharging. While the battery temporarily frees the test subjects from the constraints of a tether, battery life (without recharging) is typically limited to <48 h due to the weight/volume versus capacity limitations of current battery technologies. At this point, the researcher must again interact with the subject directly, exposing both the subject and the researcher to injury hazards and interrupting the experiments. In addition, the battery adds weight, volume, and risk of harm to the subject due to battery cell failure resulting from electrolyte or anode breakdown.

Table 1 Comparison of State-of-the-Art Wireless Neural Recorders

	Borton et al., 2013 [21]	*Yin et al., 2014 [34]*	*Schwarz et al., 2014 [35]*	*PennBMBI, Liu et al., 2015 [18]*	*Wireless μECoG, Muller et al., 2015 [22]*	*WIMAGINE, Mestais et al., 2015 [19]*	*Ando et al., 2016 [23]*	*Su et al., 2016 [24]*	*Neural Dust, Seo et al., 2016 [33]*	*Teng et al., 2017 [25]*	*W-HERBS, Matsushita et al., 2018 [27]*	*He et al., 2018 [28]*	*FF-WINeR, Yeon et al., 2018 [29]*	*WAND, Zhou et al., 2018 [30]*	*ENGINI, Ahmadi et al., 2019 [31]*	*Neurograin, Lee, et al., 2021 [32]*	*This work, [36]–[38]*
Technology	500nm CMOS + Discrete	500nm CMOS + Discrete	Discrete	Discrete	65 nm CMOS	Discrete	180 nm CMOS + Discrete	350 nm CMOS + Discrete	Discrete	65 nm CMOS	180 nm CMOS + Discrete	180 nm CMOS + Discrete	350 nm CMOS + Discrete	180 nm CMOS + Discrete	350 nm CMOS	65 nm CMOS	Discrete
BCI Size (mm)	56 x 42 x 11	52 x 44 x 30	-[a]	56 x 36 x 13	6.4 x 6.4 x 0.7 (IC)	50 x 50 x 10	53 x 31 x 47 (Transmitter)	35 Diam x 10 H	3 x 1 x 0.8	1 x 1 (IC)	21 x 25 x 7	28 x 24 x 1.4	36 x 33 x 15	1.4 x 1.5 (IC)	4 x 4 x 1	0.65 x 0.65 (IC)	**63 Diam x 77 H**
ADC (bits)	12	12	12	12	15	12	12	16	8	-[a]	12	10	10	15	11	8	**16**
No. of Channels	100	100	512	4	64	64	4096	32	1	8	128	1	96	8	1	1	**<16**
Sampling (kSps)	20	20	31	21	1	0.8 x 32, 30 x 1	1	1	10	-[a]	0.25/0.5/1	0.5	1	25	1.6	1	**<20**
Stimulation Capability	✗	✗	✗	✓	✗	✗	✗	✓	✗	✗	✗	✓	✗	✓	✗	✓	✓
Uplink Comms Type	Conventional (FSK)	Conventional (OOK)	Conventional (FSK)	Conventional (GFSK)	Backscatter (ASK)	Conventional (Proprietary)	Conventional (ZigBee)	Conventional (μESB)	Backscatter (ASK, Ultrasonic)	Conventional (QPSK)	Conventional (802.11 Wi-Fi)	NFC ISO/IEC 1443-A (ASK)	Conventional (IR-UWB)	Conventional (BLE)	Backscatter (LSK)	Backscatter (BPSK)	**Backscatter (DQPSK, SSB FSK, or OFDM)**
RF Comms Band	3.2/3.8 GHz	3.5 GHz	2.4 GHz	2.4 GHz	300 MHz	402-405 MHz	7.9 GHz	2.4 GHz	N/A	403 MHz	2.4 GHz	13.56 MHz	133 MHz	2.4 GHz	433 MHz	915 MHz	**915 MHz and/or 2.4 GHz**
Wireless Data Rate (Mbps)	24	48	1.33	2	1	0.45	128	1	0.5	8	1.6	0.106	0.8	1.96	0.205	10	**up to 25**
Max Uplink Separation (mm)	3000	5000	10000	3000	13	2000	5000	> 10 [a]	8.8	-[a]	>25 [a]	5 [b]	2000	18	12	8	**6000[c]**
Power (mW) (Total | Per Channel)	90.6 | 0.91	61-97 | 0.61-0.97	1056 | 2.07	24.09 | 6.02	0.265 | 0.004	75 | 1.17	1376 | 0.336	41.07 | 1.28	0.12 | 0.12	5.6 | 0.70	200 | 1.56	— | ~1.8	—| <0.30	172 | 21.5	— | 0.092	— | <0.03	**342[d] | 21.4**
Comms Power (mW)| Energy Efficiency (pJ/bit)	— | —	15 | 312.5[e]	33.9[e] | 25,488	23.1 | 11,550	0.0024 | 2.4	10.5 | 21,000	561 | 4,383	15.39 | 15,390	— | —	5.6 | 700	— | —	— | —	— | —	28.8 | 14,694	— | —	— | —	**≤0.309[f] | 12.4-198[g]**
Battery Duration (h) [h]	22.7	48	24	~ 5.5	✗	✗	30	32.43	✗	429	9	✗	✗	14.66	✗	✗	**8**
Wireless Power (MHz @ Max Separation mm)	2 @ 5	✗	✗	✗	300 @ 12.5	13.56 @ 25	266 @ 25	1.056 @ 10 (Ultrasonic)	1.85 @ 8.8 (Ultrasonic)	✗	0.265 @ 25	13.56 @ 5[g]	131 @ 18	✗	433 @ 12	915 @ 8	**13.56 @ 230**

[a]Exact value not reported
[b]Approximate scalp thickness
[c]SSB FSK modulation at 1 Mbps data rate in the 2.4 GHz ISM band
[d]Sum of NeuroDisc and AIR-WPT RX power consumption
[e]TX power consumption of the nRF24L01+ at 0 dBm transmit power
[f] Measured static+dynamic power of the backscatter modulator for DQPSK modulation at 25 Mbps.
[g]12.4 pJ/bit for DQPSK modulation at 2 Mbps. 160 pJ/bit for SSB OFDM modulation at 1.25 Mbps
198 pJ/bit for SSB FSK modulation at 1.0 Mbps
[h]Duration normalized to 2.4 Wh Li-ion Battery

Key Challenge: Interactions Between RF Energy and Biological Tissue: A common challenge for all electromagnetic (EM)-based W-BBCIs is the need to provide safe power transfer and data links to circuitry within, or adjacent to, a lossy biological tissue medium. The lossy medium absorbs EM energy, and this absorption increases with frequency due to dielectric loss mechanisms [39]. The resulting penetration depth of an EM source, where the source amplitude reduces to e^{-1}, generally decreases with frequency [40]. For example, the penetration depth for brain gray matter at 13.5 MHz is ≈31 cm and at 2.4 GHz is ≈2 cm [41].

While the reduction in end-to-end efficiency of the wireless power or data link at high frequencies significantly impairs wireless connectivity, tissue absorption also results in heating due to the fields surrounding the transmit (TX) and receive (RX) antennas [42]. Specific absorption rate (SAR) is a key metric for RF energy absorption in tissue and is regulated by government regulatory bodies, such as the U.S. Food and Drug Administration (FDA), the Occupational Safety and Health Administration (OSHA), the Federal Communications Commission (FCC), and their international equivalents. The IEEE and other standards bodies, such as ICNIRP, recommend SAR limits for the general public to be 0.08 W/kg as a whole body average and 2–4 W/kg for localized SAR in the head/trunk and limbs from 100 kHz to 6 GHz [43].

SAR can be calculated as $\text{SAR} = (1/V)\int(\sigma(r)|E(r)|^2)/(\rho(r))dr^3 \approx c_p(\Delta T)/(\Delta t)$, where $\sigma(r)$ is the electrical conductivity of the tissue, $E(r)$ is the rms electric field inside the tissue, $\rho(r)$ is the tissue density, V is the volume of the tissue, c_p is the specific heat capacity of the tissue, ΔT is the change in tissue temperature, and Δt is the change in time under the condition that Δt is much less than the time constant of thermal conduction and convection (due to blood perfusion). Knowing the average properties of the subject's biological tissue allows one to computationally model and simulate absorption as a function of device placement within the tissue. Direct measurement of absorption and consequent heating is also possible with the aid of a tissue phantom that mimics the part of a subject's human or animal body [44].

At a given tissue depth, the internal induced electric field (E_i) and, in turn, induced current increase as frequency decreases. In addition to the heating effects described by SAR, high E_i can result in stimulation of excitable tissue resulting in randomized APs. The possible damage to biological tissue resulting high E_i is regulated by the same bodies mentioned above to 135 f V_{rms}/m at 0.003–10 MHz for the general population [45], where f refers to the frequency of operation. While the above hazards are most severe for subcutaneous (implanted) devices, the same hazards also apply to the volume of tissue surrounding externally attached devices in the presence of strong EM fields.

Fundamentally, reduction of SAR can be achieved by a combination of careful choice of operating frequency, TX/RX antennas, and surrounding materials. In addition, minimizing the required RF power carried by a wireless power system and/or needed for wireless data transfer also has the effect of minimizing SAR. Thus, improvements in wireless power transfer (WPT) efficiency and improvements in the power efficiency of the BBCI device both have significant benefits for RF hazard reduction.

B. Wireless Power and Data Transfer Approaches Enabling Perpetual Operation

By continuously supplying the required power to the BBCI wirelessly, or by intermittently charging an onboard battery that supplies power when the subject leaves the active charging zone, a BBCI can operate wirelessly, effectively in perpetuity. In Table 1, most of the W-BBCI systems that have WPT capability employ NRIC though power transfer via ultrasonics (US) [24], [33] and far-field EM coupling [32] are highlighted as well. Of the three WPT modalities, US can provide the highest link efficiency versus separation of TX to implanted RX, with the smallest required form-factor due to the short wavelength of US energy in aqueous tissue. However, the ultrasonic transmitter requires epidermal contact, the power transfer efficiency (PTE) is highly sensitive to misalignment and changes in intervening tissue properties, and the long-term safety of chronic US power transmission is still unknown. While NRIC allows for relatively high PTE for intermediate separations between transmit (TX) coil (TXC) and receive (RX) coil (RXC), for a noncontinuous intervening medium between the two, and for greater misalignment tolerance, the RXC has a larger minimum form-factor than that required by US, and greater care must be paid to comply with regulatory SAR limits. Finally, though FF allows for considerably smaller RX antenna form factors and longer transmission distances in the air, when transmitting through tissue, the same SAR concerns from NRIC WPT apply to FF. In addition, due to higher rectification losses and tissue absorption at GHz frequencies, in order to even achieve moderate PTE, the RX system power requirements must be low (<5 mW), and the implant depth must be shallow (<10 mm) [46], [47]. For all of these WPT modalities, having a low power RX (WPT controller + communication + neural recorder) eases the energy delivery demand by the transmitter, which, in turn, lowers the effect of SAR heating and transmitted noise.

Another critical challenge with W-BBCIs is implementing an energy-efficient wireless uplink. In many cases, the power consumption of the wireless uplink dominates the power budget. In nine out of 11 designs examined in [48], the radio was the most power-hungry component on the W-BBCI, far exceeding the data acquisition (neural signal amplification and analog-to-digital conversion) stages. Power savings in the wireless uplink, therefore, offer a significant advantage to the complete power budget of the W-BBCI. Reducing the per-bit energy expenditure can enable a longer duration of operation for a given amount

of stored energy while enabling smaller form-factors. It can also help to reduce thermal dissipation and coupled noise in the system. Wireless, ultralow-power backscatter communication is a potential alternative to conventional radios in certain applications. By repartitioning the power-hungry amplifiers and RF carrier wave (CW) generators of conventional radios to a less-constrained external system, backscatter radios can achieve significant energy savings. Backscatter radios have been shown to achieve megabit per second (Mb/s) data rates while consuming microwatts of power, yielding per-bit energy efficiencies on the order of pJ/bit [36], [37], [49]–[51] and a 50–1000X improvement versus conventional radios, such as Wi-Fi [52] and Bluetooth Low Energy (BLE) [53].

C. Enabling Freedom of Movement via Wireless BBCIs

To provide for long-duration operation of these W-BBCI for free-moving animals, numerous cage-based systems employing variations on NRIC WPT and far-field UHF data transfer have been developed. For low-power neural recording devices carried by small animals (e.g., rodents), significant effort has been put into developing WPT-compatible cages using overlapping arrays [54]–[58] or cavity resonator-based magnetically coupled systems [59]. A review of wirelessly powered cages for freely moving experiments with small animals is provided in [60].

These systems are predominantly oriented toward rodent-sized home cage dimensions (20 × 23 × 45 cm) and are intended to provide <100-mW power at up to 60% PTE. More recently, conductive contact with the cage floor has been used to transfer <50 mW [61]. However, these systems will not provide the power required to recharge the batteries that would be needed for larger, nonstationary animals, such as an NHP. Standard NHP cages are built of stainless steel for mechanical strength and ease of cleaning in an autoclave. Their metallic walls form a reverberant cavity at commonly used communication frequencies (e.g., the UHF and microwave bands), resulting in dense multipath within the cage and deep nulls occurring only a few centimeters apart [62]. To address this limitation of metal cages, custom nonconductive cages [63], [64] have been developed to allow unimpeded recharging of wireless devices. Such custom animal housing solutions would be a prohibitive change for NHP labs where the costs to replace the current, USDA Animal Welfare Act approved housing would be significant and require additional upkeep and maintenance. As an alternative to modifying the cage, a mode-stirring technique leveraging switched parasitic antennas mounted to existing cage walls has been developed to create a more favorable wireless channel by reducing destructive interference [65].

By combining the power savings of backscatter communication with NRIC WPT, a W-BBCI can continually cycle through short charging and long operational phases without significant interruption. For high data rates required by modern high-channel count neural recording devices, and for TX antenna to RX antenna orientations and distances that can support freely moving animal behavior, systems employing backscatter communication will greatly benefit from the power-efficient wireless link. At the relatively high power required by high channel count and high data rate wireless neural recorders, NRIC allows for a >10× improvement in efficiency compared to FF, or nonresonant modalities, and has less dependence on the transmitter to receiver orientation, or intervening medium, than US [47]. With appropriate feedback control between the RX and TX systems, this PTE can then be traded off for expanding the TXC to RXC separation and allowing for coil misalignment while still keeping the transmitted power low. In addition, by relying on the magnetic field to transfer power near or within biological tissue, which has relatively low permeability [39], NRIC WPT causes less heating than methods that rely on the electric field to deliver the same amount of power [66]. These benefits make the combination of backscatter communication and NRIC WPT an appealing choice for new W-BBCIs.

III. KEY DESIGN CONSIDERATIONS FOR WIRELESS BBCIs

Many W-BBCIs have been developed for use in freely moving animals, e.g., [6], [16]–[32], [34], [36], and [68]. A common limitation of these existing systems has been operational durations generally ≪48 h. We present advancements in adaptive inductive resonant wireless power transfer (AIR-WPT) and wireless backscatter communication that could enable long-duration W-BBCI operations by combining long-distance wireless charging with significantly reduced power consumption on the BBCI (see Fig. 2).

A. Frequency Selection for Wireless Power Transfer

A minimum between regulatory defined maximum permissible exposure of SAR heating and induced electric field can be found around 1.5 MHz; however, the lowest globally allocated, without local restriction, frequency allowed for medical devices, within the Industrial, Scientific, and Medical (ISM) bands, is 13.56 MHz with a bandwidth of 14 kHz [68]. While this narrow bandwidth would limit the achievable data rate for wireless telemetry, at the much higher transmitted power levels that must be used to power a device, this frequency becomes a practical target for efficient WPT. As an additional benefit of using the 13.56-MHz band, the heating of metal objects caused by magnetic fields is lower than the heating that would occur at lower frequencies because eddy current losses induced in nearby metal objects decrease with the square root of the frequency increase [69]. This benefit is important

as there are therefore fewer constraints on encapsulation materials for the BBCI.

B. Frequency Selection for Wireless Communication

The choice of a particular frequency band for wireless communications is influenced by tightly coupled considerations. For the W-BBCI, the choice of frequency directly impacts system constraints, such as available bandwidth, antenna size, radio power consumption, radio link budget (e.g., path loss which increases with frequency [70]), and SAR [36].

For research systems seeking a path toward clinical use and/or commercialization, choosing an unlicensed frequency band, such as the 915- and 2.4-GHz ISM bands, reduces any future design changes required for regulatory compliance. In addition, COTS components are generally low cost and readily available for ISM band radios due to the numerous consumer products using these bands. A drawback to using the ISM bands is the increased risk of cochannel interference from existing devices, e.g., Wi-Fi or Bluetooth-enabled devices in the 2.4-GHz ISM band. For this reason, many devices are designed to operate in the Medical Implant Communications Service (MICS) bands of 413–419, 426–432, 438–444, 451–457, or 2360–2400 MHz. The drawback of the use of the UHF MICS bands is the narrow channelization in those bands.

C. Design Requirements for Wireless Data Uplinks

High data rate wireless uplinks on W-BBCIs are motivated by the need to analyze and/or respond to precise features of neural signals as transduced simultaneously by potentially large numbers (dozens to hundreds) of electrodes. The electric fields generated by ionic channels in neurons during APs or "spikes" can be measured using COTS electronics [71], [72]. A complete AP typically lasts 1 ms, and in order to measure the dynamics of depolarization and repolarization, sample rates of $\geq$20 kHz per neural channel are needed. When measured outside of a neuron, the AP amplitudes can be on the order of 10 s of μV, typically requiring analog-to-digital converter (ADC) resolutions of $\geq$10 bits, e.g., [49] and [72].

If one considers collecting 32 channels of neural data with 16-bit voltage resolution and a sampling rate of 20 kSamples/s (kSps) per channel, the total biological data volume is more than 10 Mbits/s (Mb/s), which can grow to more than 20 Mb/s with the addition of data packet structure, error correction coding, and housekeeping information, such as timestamps. Since neural spiking data are often sparse, data compression techniques can be used to reduce the required data rate, for example, by only transmitting spike events per channel as in [67] or by transmitting the specific channels on which a spiking event occurred [48]. However, in research applications that require broadband neural data, for example, neural plasticity experiments using phase-based stimulation triggers [73], high-rate neural recording with wireless uplink rates >10 Mb/s may be required.

A conventional radio uplink can consume a significant portion of a W-BBCI's power budget even when data are compressed, as highlighted in [48]. Careful design of the wireless uplink is, thus, important for energy-constrained W-BBCIs targeting long-duration experiments. For example, an off-the-shelf Nordic Semiconductor nRF24L01+ chip can be used as a BLE link and has been used in many works, including [35]. This device consumes between 21.5 and 40.7 mW for an output power of 0 dBm, with a maximum data rate of 2 Mb/s and per-bit energy efficiency between 10 and 20 nJ/bit [53] (note that the effective data rate for transmitters can decrease by as much as 75% when packet overhead for link-layer management is considered [74]). In contrast, the power consumption of an off-the-shelf Intan Technologies RHD2132 biopotential front-end will consume 6.4 mW while recording broadband neural data (20 kSps) from six channels with 16-bit resolution, generating 1.9 Mb/s of biological data [72]. Switching to a Wi-Fi 802.11g uplink using an ESP8266EX device (Espressif Systems [52]) at 54 Mb/s would consume 420 mW or 7.8 nJ/bit. Other state-of-the-art W-BBCI systems have, heretofore, been limited by shorter operational durations or reduced uplink throughput [75].

D. Efficient, SAR-Limited Wireless Power Transfer via Near-Field Resonant Inductive Coupling

Pairing the 13.56-MHz power transmit frequency, as discussed above, with NRIC, provides the capability of delivering high PTE to W-BBCI. In the simplified diagram of a typical NRIC system shown in Fig. 2(b), an external high-power TX base station consisting primarily of an RF signal source and a power amplifier (usually Class-E to take advantage of high operating efficiency up to a few tens of MHz [47]) drives a TXC tuned to the chosen resonant frequency using an impedance matching network (IMN). A weakly coupled RXC, tuned in a similar manner to the same resonant frequency, then drives an RF rectifier to convert the ac RF signal to dc, usually a Zener diode or MOSFET-based full-wave bridge. This rectified voltage is then regulated, via up or down-converters, to the required system voltage. Energy is stored in a capacitor array or in colocated batteries. This energy is then available to drive the required load, such as the neural recording system, stimulation system, processing elements, and the wireless uplink. To maximize the mutual coupling between the TXC and RXC, the resonant system should be adjusted to resonance in an environment that mimics the intended application space, e.g., with the TXC coaxially aligned and vertically offset from the RXC within its encapsulation and intended medium.

By relying on the magnetic field that couples the TXC to the RXC to transmit power, rather than an electric field, the inductively coupled channel results in lower

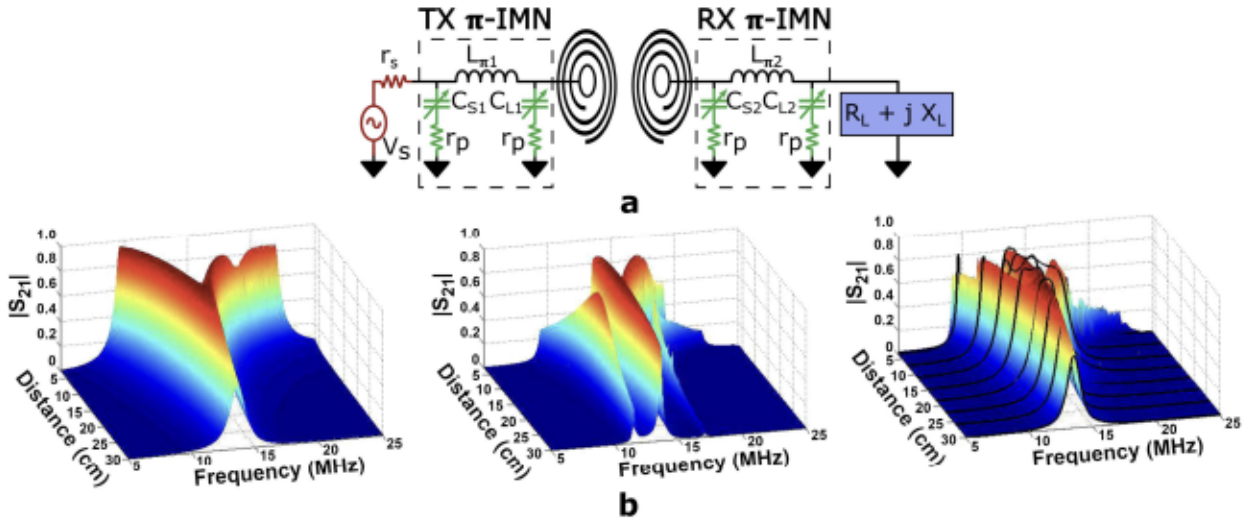

Fig. 3. *Overview of adaptive impedance network matching. (a) Block diagram of a WPT system, including an IMN, in this example, a π network. (b) Surface plots of extracted, normalized coupling $|S_{21}|$ for (left) 50-Ω source and load termination impedances, (middle) π-match network at the TX side, corresponding to the simulated ideal conjugate match algorithm, and (right) π-match network at both the TX and RX sides corresponding to a simulated parasitic optimization algorithm (surface plot) with the experimental results overlayed (black lines). (From [76], with permission.)*

SAR (lower tissue heating) and negligible channel variations due to inhomogeneous tissues since most biological materials have a permeability of approximately 1 [77]. In addition, by tuning the combined TX to RX system to a single resonant frequency, high Q-factor transmission can be achieved. This makes the coils less sensitive to misalignment and increases the PTE, as a lower transmitted power can achieve the same received power at the load, which, in turn, decreases both heating in the coil itself [69], as well as heating of the surrounding tissue.

1) Challenges for Near-Field Resonant Inductive Coupling: Optimally tuned NRIC WPT for low-power wireless medical devices (tens of mW) within constrained application spaces can achieve end-to-end efficiencies approaching 60% [47]. The key characteristics of the application space that drives the design include whether the separation, alignment, and orientation of the coupled resonators are fixed or variable; adapting to the TX switching amplifier output impedance; and adapting to the RX load impedance. When these characteristics change, the PTE for the previously optimal set of IMNs changes as well, likely resulting in reduced efficiency. Within the SAR limitations on field strength [78] and within the stable operation of the switching amplifier, the output power can be scaled to compensate for the PTE loss with closed-loop control between the TX and RX. Alternatively, in order to maintain high PTE in this expanded application space, either the operating frequency can be adjusted to the new optimal frequency [79], [80] or the impedance of the IMNs can be adaptively controlled [76], [81]. Tuning the operating frequency may exceed the available bandwidth allowed by a given regulatory jurisdiction, or interfere with other devices, especially within medical environments. Adjustable inductances are typically large, low-Q, and coarsely quantized, so adjusting the capacitance within the legs of π-match topology IMNs [see Fig. 3(a)] is preferable [76]. As shown in Fig. 3(b), with fine enough control over the IMNs, the frequency splitting resulting from overcoupling as the RX approaches the TX can be adaptively reduced such that a near-constant optimum $|S_{21}|$ can be achieved for a wide range of distances. While matching on both the RX and TX broadens region of optimal $|S_{21}|$, for W-BBCI, the RX is usually also volume constrained, so the receiver may have only a few coarsely spaced adjustable capacitances available.

Adaptive tuning typically improves the efficiency of NRIC systems when high power (more than, e.g., 100 mW) is to be transferred additional difficulties that arise. First, the American Association of Medical Instrumentation guidelines limit the allowable chronic temperature increases in the tissue to less than 2 °C [82]. In high-power scenarios, inefficient power regulation or conversion in the RX can lead to significant heat conduction into the surrounding tissue that exceeds this limit. Second, in addition to the EMI resulting from the inductive field itself, the nonlinear rectification of the RF input to the WPT RX creates harmonic energy and additional spurious frequency components that spread noise through the spectrum and can lead to significant noise on the dc power planes. This power-plane noise can be an issue throughout the device even if star-ground internal PCB plane connections are used. While many consumer electronic devices are relatively tolerant of power supply noise, neural recording devices are designed to amplify weak neural signals, and they are, therefore, extremely sensitive

to power supply noise due to common-mode rejection ratio (CMRR) limitations.

IV. EMERGING APPROACHES FOR WIRELESS BBCIs: IMPROVED WIRELESS POWER AND DATA UPLINKS

A. Wireless Backscatter Communication for High Data Rates and Low Power Consumption

Backscatter communication is an energy-efficient alternative to the high power consumption of conventional wireless uplinks. Backscatter radios offer Mb/s data rates while consuming microwatts of power, yielding per-bit energy efficiencies on the order of pJ/bit. While commonly used in severely energy-constrained applications, such as radio frequency identification (RFID), backscatter radios have recently seen more use in wireless sensing applications. For example, backscatter communication has been used to telemeter neural data from dragonflies in flight using a battery-free neural recorder [83] and enable a battery-free wireless camera [84]. The technology has also been validated in other electrophysiology applications as well [22], [32], [36], [85].

Backscatter communication achieves high energy efficiency by redistributing power-hungry elements in a wireless link to a power-rich external system. Unlike conventional radios, backscatter-based uplinks do not require RF amplifiers and oscillators to generate a communication CW. The CW is instead provided by an external transceiver having access to, e.g., mains power or a large external battery. As shown in Fig. 2(b), a backscatter-based device can communicate data by applying a time-varying impedance to its antenna, which modulates the amplitude and phase of the incident CW. In this case, the backscatter-based device only needs to provide enough power to actuate an RF switch or a transistor, which is typically consumed microwatts rather than milliwatts. The modulated signal is then scattered by the device's antenna and received by an external system that could be a custom receiver or a commodity device, depending on the frequencies used, the modulation scheme, and the protocol. This modality allows for small-form-factor systems with high data rates (>96 Mb/s) [88] at orders of magnitude lower power consumption compared to conventional wireless standards [37], [50].

Other technologies achieve similarly high per-bit energy efficiencies, such as ultrawideband (UWB) radio [89] and ultrasound [90]. These technologies are a potential alternative to backscatter communication, but backscatter communication remains an attractive choice for brain–computer interfaces (BCIs) due to its simplicity, lower overall power consumption compared to UWB, and use of tissue-penetrating RF frequencies. Furthermore, backscatter has the potential for compatibility with existing protocols, such as BLE [37], [50], [74] and Wi-Fi [51], enabling compatibility with unmodified, COTS receivers, and reducing the complexity of the system.

An additional benefit of backscatter communication is that it can be easily implemented on a W-BBCI using all-digital components. With the use of digital logic (e.g., MCU or FPGA), an RF switch, and an antenna, it is possible to implement a backscatter uplink. Research has even shown that backscatter communication is possible by simply using existing general-purpose input/output pins of unmodified MCUs and FPGAs as the modulator [91]–[93]. The all-digital nature of backscatter communications means that devices can be prototyped with low-cost, COTS components and then relatively easily translated to a fully integrated ASIC. Even using COTS components, backscatter radios are capable of extremely efficient RF communication, as shown in Fig. 4.

While backscatter communication offers significant energy efficiency, it comes at the cost of a less favorable link budget compared to conventional radios. Because the externally generated CW travels a round trip from the external system to the backscatter radio and back, the RF path loss changes as $1/r^4$ for a backscatter system, rather than the usual $1/r^2$ for conventional radios, where r is the free-space distance between the external system and the BCI antenna [94], [95]. Given the round-trip nature of the backscatter link budget, multipath interference can significantly reduce the reliability of backscatter radios. This is particularly important within metal animal cages where deep nulls can form in the channel transfer function [62]. For experiments conducted inside the cage of a freely moving animal, the multipath environment could result in dropped data. Careful attention to the communication channel and the link budget design are, therefore, required to ensure reliable communication.

An example of a wirelessly charged, backscatter-based BCI device is the *NeuroDisc* [36]. The NeuroDisc is a wireless neural recording tool for researchers, which uniquely synthesizes previous advancements in low-power backscatter communication and biological sensing to reduce the power burden of wireless uplinks on neural recorders. The NeuroDisc is differentiated from other wireless neural recorders by an FGPA-based reconfigurable backscatter uplink that enables the use of several different ultralow-power communication modes from a single hardware platform: a 25-Mb/s DQPSK uplink using a custom protocol [36] can transmit large volumes of data, as needed for broadband neural recording; a single sideband (SSB) BLE compatible frequency-shift keying (FSK) uplink [37], [74], [96] that facilitates the integration of the NeuroDisc with unmodified COTS receivers; an orthogonal frequency division multiplexing (OFDM) backscatter uplink [38] that could eventually provide greater resilience to multipath fading observed in animal cage environments.

To measure neural signals, the NeuroDisc uses a low-power Intan RHS2116 electrophysiology interface that can sample 16 channels at 20 kSps with 16-bit resolution,

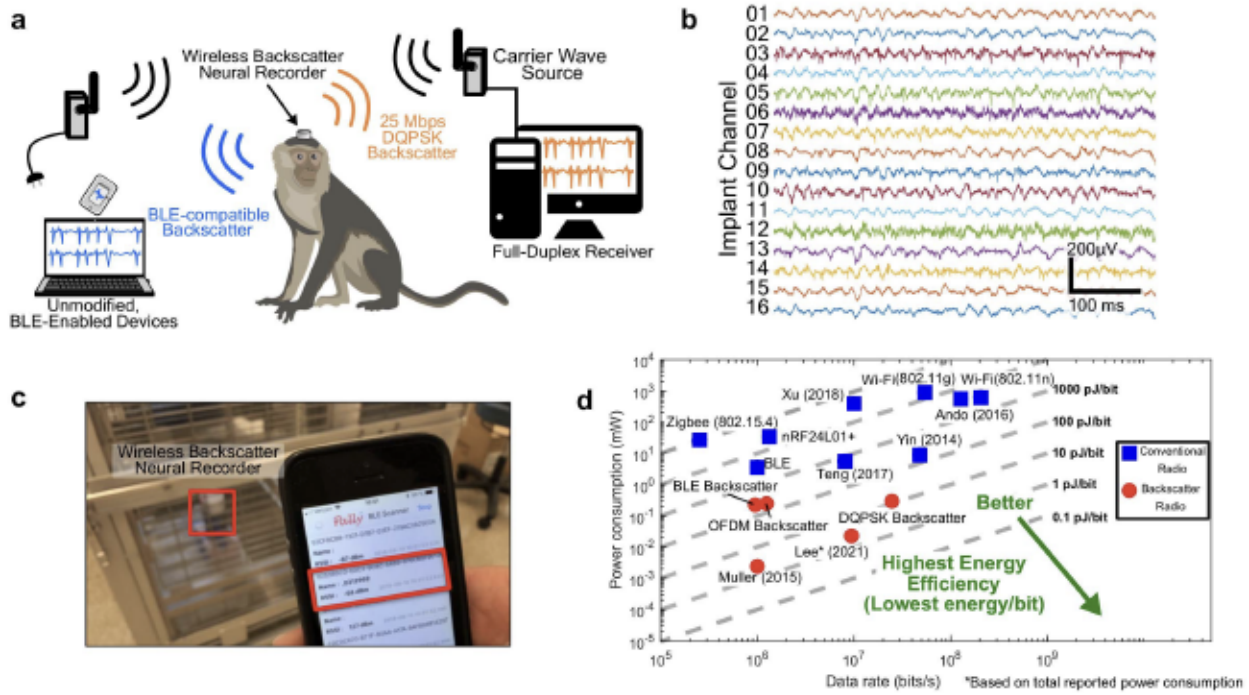

Fig. 4. *Backscatter-based wireless uplinks can be used for diverse modulation schemes and uplink modalities. (a) Diagram illustrating the multimode, multiband capability of backscatter communication. (b) Neural recordings uplinked from an anesthetized NHP using a 25-Mb/s differential quadrature phase shift keying (DQPSK) backscatter uplink. (c) Photograph of BLE backscatter packets being received from outside an NHP cage on a smartphone using the same wireless neural recorder as in (b). (d) Per-bit energy comparison of selected state-of-the-art radios. In general, backscatter radios achieve the highest energy efficiency. Figures are adapted from [37], [87], and [88].*

allowing recording and uplink of low-frequency LFPs and high-frequency neural spikes [72]. The RHS2116 also provides stimulation capability, enabling eventual use in recording and stimulation experiments. The full signal chain of the NeuroDisc has been validated through *in vivo* experiments, as shown in Figs. 4 and 5. The NeuroDisc was connected to a chronically implanted Utah Array (Blackrock Neurotech) and operated on battery power without the use of WPT. The 25-Mb/s DQPSK backscatter uplink was used to transmit measured broadband neural activity to a full-duplex receiver based on a software-defined radio [36]. The *in vivo* experiments were performed at the Washington National Primate Research Center, Seattle, WA, USA, and all experimental procedures were approved by the University of Washington Institutional Animal Care and Use Committee.

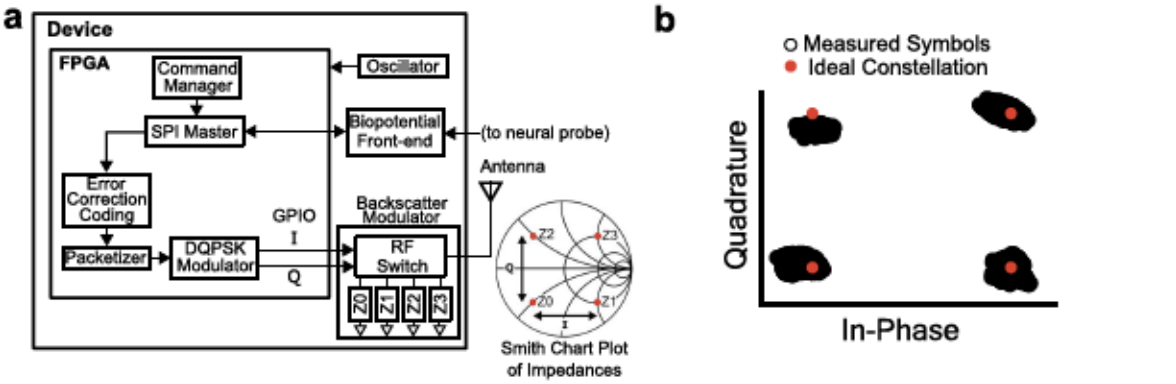

Fig. 5. *Example implementation of a DQPSK backscatter uplink. (a) Block diagram illustrating the fully digital logic and RF switch used as a backscatter modulator. Impedances Z0–Z3 are chosen to yield four constellation points of the same magnitude 90° phase offsets. (b) Measured signal constellation at the receiver compared to the ideal constellation. Figures are adapted from [36].*

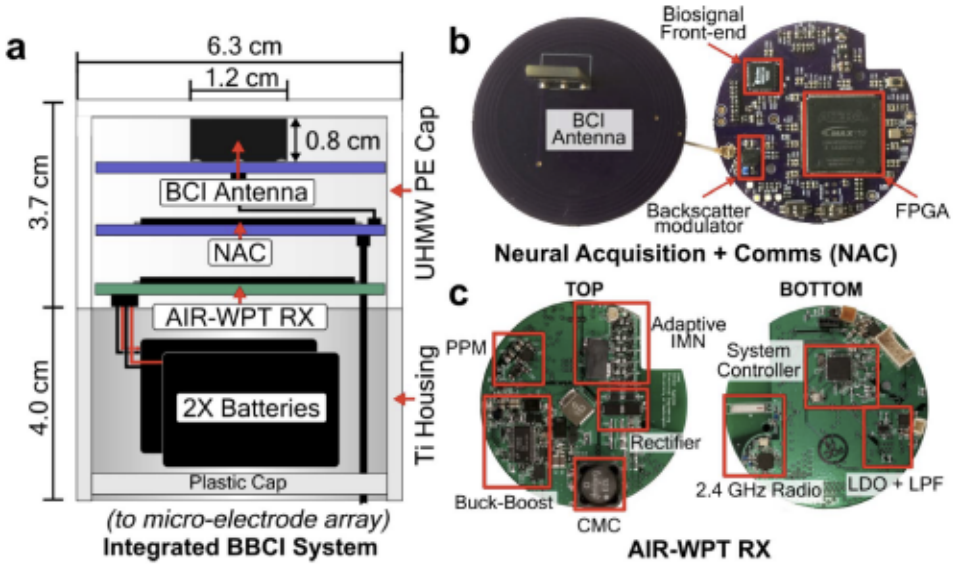

Fig. 6. *Prototype of a Perpetual W-BBCI. (a) Illustration of the integrated system composed of (b) dual-band BCI antenna [62] for data and power and the Comms FPGA for high-rate electrophysiological signal acquisition, processing, and uplink, and (c) AIR-WPT receiver (AIR-WPT RX).*

B. Transmitters and Receivers for Adaptive Inductive Resonant Wireless Power Transfer

The AIR-WPT TX and RX shown in Fig. 7, with the RX implemented as in Fig. 6(c), were developed to perpetually and safely power BBCI devices over ≈10–50-cm TXC to RXC separations within a caged environment. This enables freer movement of the NHP subject within their home cages. The primary constituent blocks are an adaptive impedance match for efficient power transfer, a bridge rectifier with a storage capacitor rated for a breakdown voltage of 50 V to handle large swings in the unregulated rectified voltage, a buck–boost converter that regulates down to 4.2 V required for Li-Ion battery charging, a low-noise voltage regulation block to provide a 3.3-V rail to the BBCI electronics, and a power management microcontroller that controls the operation of these blocks and communicates with the external power transmitter via a low-rate 2.4-GHz radio.

A typical usage model for the AIR-WPT system has the TXC positioned in the back-left corner of the NHP cage at a location above the NHP's seat perch, as shown in Fig. 9(a) and (b), where the NHP typically chooses to go for rest and sleep periods. The TX resonator is driven by a Wibotic Inc. WRELv2 transmitter [97] located outside the cage. While the NHP is in this position, the RX's battery is recharged. Typically a pair of 3.7-V 3500-mAh Li-Ion batteries are used as shown in the stackup of Fig. 6(a).

C. Closed-Loop Control of the WPT Link

The safety of test subjects is a critical concern in animal studies. Beyond the SAR and conductive heating due to high TX power and inefficient RX populated component operation, an onboard supervisory controller must also guard against high humidity, electrical shorts, and battery cell failure. To accomplish this, the controller must monitor the board temperature and current loads, the battery cell health, and the temperature and humidity within the enclosure environment. If any of these parameters approaches the cautionary values, the controller lowers the transmitted power. If safe limits are exceeded, the transmitter senses the fault and shuts down.

D. Maintaining High SNR During Neural Recording

While the SNR of the recorded data depends heavily on the neural recording device and the communication fidelity, the expectation is that a low-noise power plane is available to power these devices. Without proper power conditioning, high-power RF transfer between the WPT TX and RX considerably increases the shared power plane noise and may, thereby, corrupt the neural recording. The noise coupled to the power plane has both a radiated EMI and conductive component. To minimize the radiated component, the neural recorder and communication subsystems can be encapsulated within thin mesh metal shielding to separate them from the power electronics. To reduce the conducted interference, the AIR-WPT RX shown in Fig. 7 was designed with a common-mode choke on the rectified output from the diode bridge rectifier. A dc switch called a "Powerpath Manager" (PPM) was used to ping-pong between two batteries, Battery A and Battery B, so that the BCI electronics were powered from one battery, while the other was charging.

As shown in Fig. 7(b), the addition of the dual-battery PPM greatly reduces the noise on the power plane for

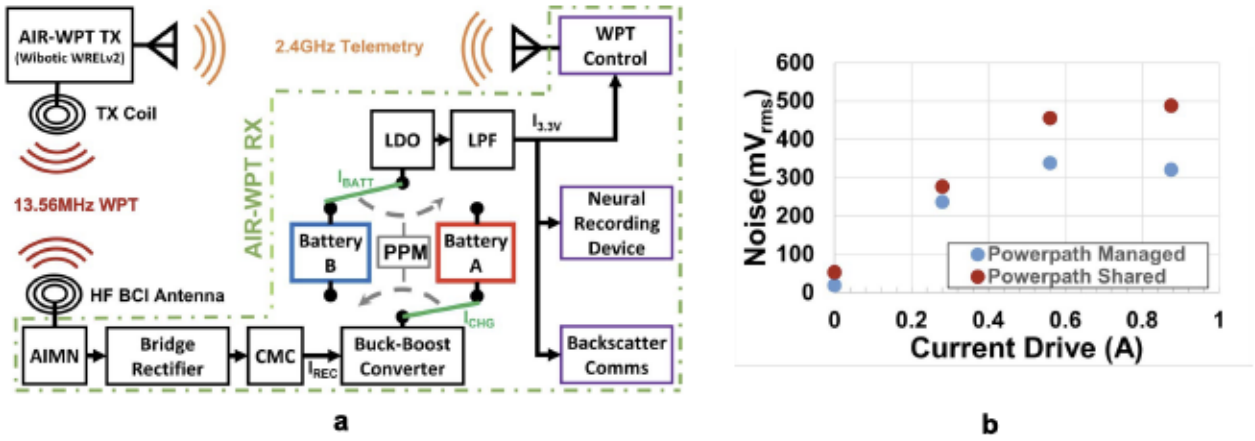

Fig. 7. *AIR-WPT system. (a) AIR-WPT system block diagram showing AIR-WPT TX, which provides both power at 13.56 MHz and bidirectional telemetry at 2.4 GHz, and the AIR-WPT RX, which adaptively matches the input impedance and conditions the input power in order to produce a low-noise 3.3-V power supply for BBCI device. (b) At a high charging current, the inclusion of a PPM decreases the noise voltage on the power plane by 35%.*

high charging rates compared to an RX that charges and provides power on the same conductive plane with a single battery. The prototype device supports a battery charging current of up to 875 mA but with excessive noise in the recording system at the highest charging current. We observed that a charging current of up to ~250 mA could be supported with acceptable noise levels during neural recording.

The safe charging of Li-ion batteries requires a multistage charging cycle that includes supplying charge in the constant current mode at the charge rate recommended by the manufacturer until the voltage reaches the max cell voltage and then, in the constant voltage mode, holding the voltage there until the current reduces to ≈(1/10) the charge rate. Fig. 8 shows measured data from a ping-pong charging system for Li-ion batteries while in operation over

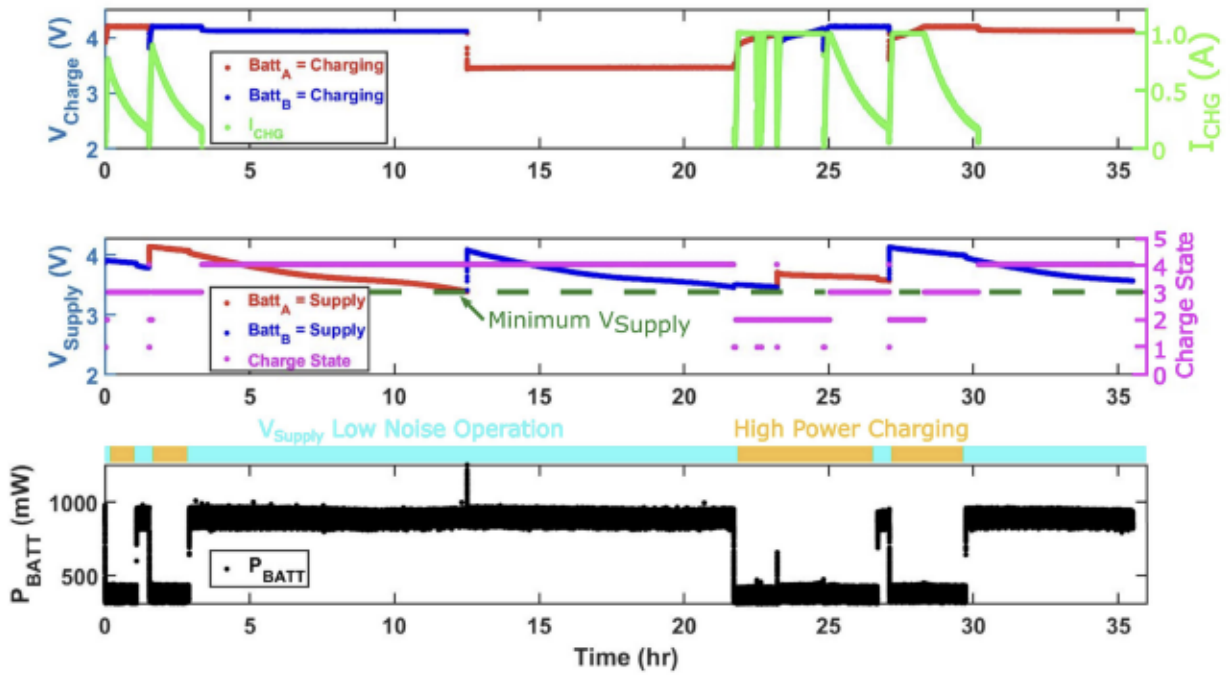

Fig. 8. *Adaptive power management example: A 35-h run demonstrates the possibility of perpetual charging and low-noise operation via time multiplexing between the charging and recording periods. The charging states 1–4 (represented by the height of the magenta trace) correspond to the precharge, constant current, constant voltage, and standby states for the Li-ion battery. States 0 and 5 correspond to error conditions, which were not observed during this run.*

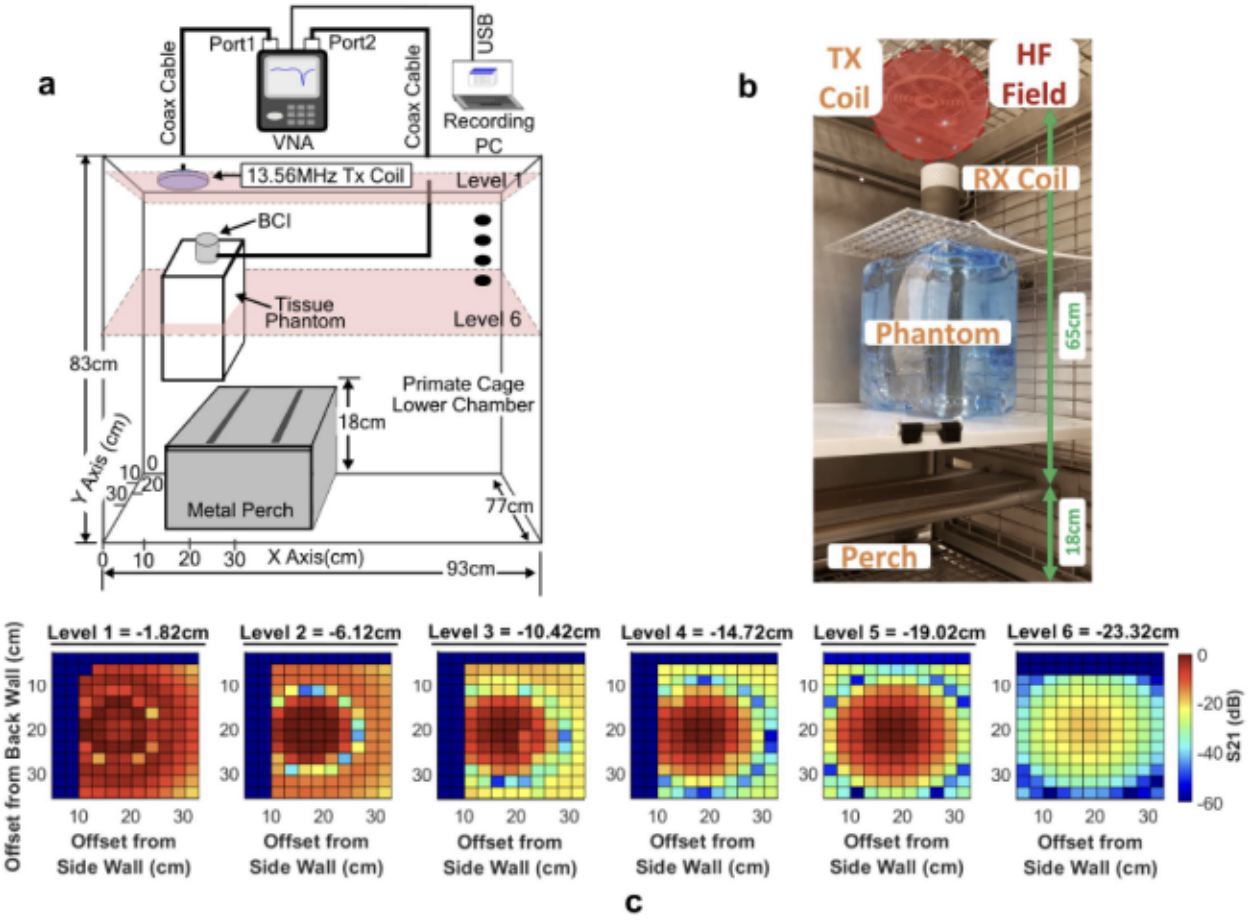

Fig. 9. *(a) Overview of the HF field characterization test setup within the lower chamber of a primate cage. The coil-to-coil insertion gain (S_{21}) was measured between the TX coil and the BCI antenna for six height levels. (b) Photograph of the test setup. (c) Field characterization between a TX mounted to the back-left ceiling of the cage and a mobile HF BCI antenna. The dark blue locations show where the antenna could not be positioned due to mechanical interference.*

a 35-h run time with an example BCI system based on the Neurochip 3 BCI device [6].

The AIR-WPT RX controller steps each battery through precharge and impedance match, constant current (∼1.1 h), constant voltage (∼1.9 h), and standby states, while the second, charged battery supplies a filtered 3.3 VDC to the noise-sensitive devices. Note that, when the charging current dropped below ∼250 mA for either battery, the system is operating in a low interference condition, so the controller powers up the neural recorder and backscatter communication systems simultaneously. This time multiplexing is best seen in the bottom plot, where the power is only delivered to the neural recording and backscatter communication systems simultaneously when the above conditions are met.

With this time-multiplexed charging system implemented, the above tested W-BBCI system requiring 958 mW could run 2.5 h for every 1 h of charging, with a maximum continuous operational period of 19 h. However, the continuous operation would be feasible if the backscatter-based NeuroDisc BCIs were used instead of the power-hungry Neurochip 3.

E. WPT Field Characterization in the Animal Cage

To better understand the limitations of WPT within a cage environment, the coupling between a TXC and an RXC [98] was measured inside an actual primate cage [99]. The TXC was mounted to the back-left ceiling with a durable plexiglass sheet. The RXC was mounted on a 7-kg Macaque phantom made from a thin plastic container filled with phosphate-buffered saline. The walls of typical NHP cages are predominantly constructed with metal mesh for durability and to allow easy cleaning in an autoclave, so the cage assembly is effectively a Faraday cage at the 13.56-MHz WPT operating frequency. Fig. 9 shows the measured mutual coupling (as indicated by $|S_{21}|$) between the TXC and the BCI antenna as measured by a VNA. For a transmitter limited to 250 W, such as the commercially available Wibotic OC-251, and a receiver that requires approximately 5 W to charge the 3.7-V battery at a max rate of 1 A, as seen in the resulting Fig. 9(c), the maximum charging rate can be achieved in the regions where S_{21} is greater than −17 dB. This maximum charging rate condition can be met for many positions (as shown in

red in the plots of Fig. 9) near the first five levels of the cage.

F. AIR-WPT RX Control Strategy

In general, recharging should be completed in the minimum time possible to maximize the interference-free data acquisition periods. This generally means that sufficient transmitted power should be available in order to charge the battery up to its charging current limit. In concert with concerns for safety, the recharging should dynamically optimize for as many TXC to RXC coupling changes as that might result from a changing RX load and changes in the TXC to RXC separation, orientation, and alignment. The RX load can change due to the charging state of the battery or the operational modes of the power plane-dependent devices (e.g., neural recorder and communication device). The TXC to RXC separation, orientation, and alignment changes result from the mounted RX system moving with the NHP. In order to remain within SAR limits and minimize the power plane noise, the optimal PTE at the lowest possible TX output power required to charge the batteries in a given time is dynamically set. To accomplish this goal, the AIR-WPT RX's responsive RX-based controller adaptively controls the TX power output and adaptively tunes a capacitive IMN, as shown in Fig. 3(a).

V. FUTURE WORK

The development of a W-BBCI using backscatter communication and NRIC WPT presents several interesting paths for future work. These include short-term objectives, such as integrated system testing en route to *in vivo* validation of a head-mounted device, as well as exploring smaller, integrated solutions for implantable devices.

A. Migrating From COTS Components to an Application-Specific Integrated Circuit

A key step for minimizing the SWaP of the BBCI device is to integrate as much of the system onto a single chip as possible. At a minimum, the digital portions of the device can be easily integrated into an ASIC. The DQPSK, BLE-compatible FSK, and OFDM backscatter modulations discussed in Section III were all implemented as fully digital designs on COTS FPGAs, while the AIR-WPT digital control was implemented in a microcontroller that could easily be instantiated within an ASIC. We expect that the total power consumption of the backscatter uplink and AIR-WPT controller would consume on the order of 100 s of microwatts or less, including backscatter modulation and digital packet handling. Further size reduction could be achieved by using inductor-free impedance constellations explored in [50] and [102]. Paired with advancements in conformable electronic interfaces, such as soft electrocorticography (ECoG) arrays, a single chip solution could enable high-resolution monitoring of neural systems in stable, minimally invasive packages.

B. Improving Receiver Sensitivity by Reducing Carrier Wave Interference

A key approach to improving the reliability of backscatter communication systems is to reduce the interference caused by the external CW at the receiver. Whether the CW is in-band as with the DQPSK uplink in [36] or out of band as the BLE NeuroDisc uplink in [32] and [38], reducing the strength of the unmodulated CW can improve receiver sensitivity and packet success rate [101]–[103]. The sensitivity of backscatter receivers can be improved by using self-jammer cancellers, which removes the unmodulated CW from the backscattered signal by adding a phase-shifted and attenuated version of the local CW. A challenge is that the movement of the W-BBCI in freely moving animal experiments introduces phase shifts in the received signal, detuning the self-jammer canceller. Adaptive self-jammer cancellers could be used to overcome this problem and improve the reception of backscattered signals.

C. Multiple Access Protocols to Support Simultaneous Streaming From Multiple W-BBCIs

Future deployments of W-BBCIs using backscatter communication will likely need to support use on multiple animals in the same environment and wireless channel. Multiple access protocols for backscatter communication are an active area of research, particularly for RFID applications. For W-BBCIs, time-division multiple access (TDMA) was recently explored for the *Neurograins* in [32] due to challenges with tuning individual devices and the limited bandwidth of the complete three-coil system. An issue with TDMA approaches, though, is the reduced spectral efficiency and, therefore, lower overall data throughput for a given bandwidth. Wideband systems leveraging frequency division multiplexing or OFDM backscatter communications, such as the all-digital OFDM backscatter architectures presented in [38], could realize greater spectral efficiencies for backscatter-based W-BBCIs.

D. Noise Reduction Options for the WPT System

Due to the high currents required to rapidly charge high-capacity batteries, conductive and inductively or capacitively coupled noise can easily interfere with the weak neural signals. These noise issues have been observed in this work and [104]. To mitigate the effects of WPT-induced noise, multiple avenues could be pursued.

1) *Adaptive WPT artifact cancellation:* At low levels of artifact amplitude with respect to the dynamic range of the recorder, i.e., those that do not saturate the neural recorder front end, the artifacts could be canceled through the application of a self-trained digital filter that learns and removes the noise signature.

2) *WPT feedforward cancellation:* With the primary noise source known, feedforward cancellation could provide power supply noise rejection that is stable for a wide array of supply currents.
3) *Rectifier interference optimized waveforms:* The noise signature could be compensated for by a TX system capable of producing arbitrary optimized waveforms to suppress interference caused by the nonlinear rectification. The rectification products (i.e., the interference signal) would be canceled by this signal.

E. Thermal Improvements

Depending on the specific components used (i.e., rectifier, dc/dc regulator, discrete components along the WPT input path, and battery pack), circuit temperature rise could exceed the permissible level of 2 °C [82]. Designers should pay careful attention to characterize thermal paths between the circuits, batteries, and tissue in order to understand potential tissue heating. Heat generation should also be analyzed in all of the systems' operating modes, including when the batteries are being charged and discharged. Accurately predicting temperature rise is very difficult, since it arises from the interaction of many factors, including circuit design, the operating modes and operating points of the circuits, and the rate at which the subject's body dissipates heat. Therefore, measuring temperature and implementing safety interlocks to prevent overheating are recommended for W-BBCI systems.

F. Large Volume Field Coverage

Increasing the working volume for wireless charging can potentially improve the performance of the system and improve the quality of life for patients. One potential approach to increasing charge volume is to use an array of switchable resonators that can route power within a large area [57], [105].

VI. CONCLUSION

This article summarizes recent progress in wireless power and communication for enabling freer movement of BBCIs that record and/or stimulate the brain. While most existing W-BBCIs have relied on batteries that must be removed and recharged externally or could only be wirelessly recharged at very close separations $\ll$10 mm between the TX and RX systems, these paradigms would heavily constrain long-duration NHP-based neural research. In this article, we highlight several of the key issues arising when applying WPT and wireless communication to BBCIs.

For the high-resolution sampling applications required for AP neural recordings, we highlight an approach using backscatter communication to improve the wireless throughput of a W-BBCI while maintaining high energy efficiency. This technique was demonstrated *in vivo* to stream 16 channels of neural data at 25 Mb/s from the primary motor cortex of anesthetized rhesus macaque using the 915-MHz ISM band at a distance of 35 cm. The per-bit energy efficiency of the backscatter modulator was measured to be 12.4 pJ/bit, which is nearly 100$\times$ lower than comparable off-the-shelf solutions (e.g., Wi-Fi and Bluetooth) achieving similar data rates.

NRIC WPT enables W-BBCI to be recharged with more positional freedom than alternative WPT paradigms. The steel cage of an NHP is presented as an environment where that positional freedom will allow for long-duration (potentially perpetual) neural recordings to be conducted. Characterizations of the field within a metal cage demonstrate practical coverage for NHP mounted system charging. The further challenges of high-power charging causing interference with neural recording motivate the creation of the AIR-WPT RX with appropriate shielding, filtering, powerpath management, and time-multiplexing of power delivery in order to mitigate the interference. Using this RX, safe, long-duration operation of a nonpower optimized W-BBCI system is demonstrated providing 2.5 h of operation for every 1 h of charging.

Finally, further research opportunities for mitigating the numerable challenges of operating a W-BBCI in caged environments are presented in hopes of eventually providing a more perfect research platform for advancing the development of personalized, networked healthcare for neurological disorders. ■

Acknowledgment

The authors would like to thank the PROCEEDINGS OF THE IEEE reviewers for their helpful feedback. They would also like to thank Profs. Eberhard Fetz, Steve Perlmutter, and Azadeh Yazdan, as well as Toni Haun, and the Staff at the Washington National Primate Research Center for supporting the data collection described in this article. All *in vivo* experiments were performed at the Washington National Primate Research Center, Seattle, WA, USA, and all experimental procedures were approved by the University of Washington (UW) Institutional Animal Care and Use Committee. Disclosure: Joshua R. Smith is a Co-Founder of Wibotic Corporation, serves on its board of directors, and owns equity in the company.

REFERENCES

[1] College of Fellows, American Institute for Medical and Biological Engineering, "Medical and biological engineering in the next 20 years: The promise and the challenges," *IEEE Trans. Biomed. Eng.*, vol. 60, no. 7, pp. 1767–1775, Jul. 2013.

[2] J. C. Kao, S. D. Stavisky, D. Sussillo, P. Nuyujukian, and K. V. Shenoy, "Information systems opportunities in brain–machine interface decoders," *Proc. IEEE*, vol. 102, no. 5, pp. 666–682, May 2014.

[3] D. Yeager, "Wireless neural interface design," Ph.D. dissertation, Dept. EECS, Univ. California at Berkeley, Berkeley, CA, USA, 2014.

[4] C. Lu *et al.*, "Flexible and stretchable nanowire-coated fibers for optoelectronic probing of spinal cord circuits," *Sci. Adv.*, vol. 3, no. 3, Mar. 2017, Art. no. e1600955.

[5] A. Jackson, J. Mavoori, and E. E. Fetz, "Long-term motor cortex plasticity induced by an electronic neural implant," *Nature*, vol. 444, no. 7115, pp. 56–60, Nov. 2006.

[6] L. E. Shupe *et al.*, "Neurochip3: An autonomous multichannel bidirectional brain-computer interface for closed-loop activity-dependent

stimulation," *Frontiers Neurosci.*, vol. 15, p. 1021, Aug. 2021.

[7] A. Mamatkulov, "Deep brain stimulation for Parkinson's disease using motor cortex sensing," *Parkinsonism Rel. Disorders*, vol. 79, pp. e15–e16, Oct. 2020.

[8] G. K. Anumanchipalli, J. Chartier, and E. F. Chang, "Speech synthesis from neural decoding of spoken sentences," *Nature*, vol. 568, no. 7753, pp. 493–498, Apr. 2019.

[9] F. B. Wagner *et al.*, "Targeted neurotechnology restores walking in humans with spinal cord injury," *Nature*, vol. 563, no. 7729, pp. 65–71, 2018.

[10] J. Abelson *et al.*, "Deep brain stimulation for refractory obsessive-compulsive disorder," *Biol. Psychiatry*, vol. 57, no. 5, pp. 510–516, 2005.

[11] J. L. Collinger *et al.*, "High-performance neuroprosthetic control by an individual with tetraplegia," *Lancet*, vol. 381, no. 9866, pp. 557–564, Feb. 2013.

[12] C. Pandarinath *et al.*, "High performance communication by people with paralysis using an intracortical brain-computer interface," *eLife*, vol. 6, Feb. 2017, Art. no. e18554.

[13] N.-R. Bin *et al.*, "Continuous monitoring via tethered electroencephalography of spontaneous recurrent seizures in mice," *Frontiers Behav. Neurosci.*, vol. 11, p. 172, Sep. 2017.

[14] S. Zanos, A. G. Richardson, L. Shupe, F. P. Miles, and E. E. Fetz, "The Neurochip-2: An autonomous head-fixed computer for recording and stimulating in freely behaving monkeys," *IEEE Trans. Neural Syst. Rehabil. Eng.*, vol. 19, no. 4, pp. 427–435, Aug. 2011.

[15] R. D. Estep, I. Messaoudi, and S. W. Wong, "Simian herpesviruses and their risk to humans," *Vaccine*, vol. 28, pp. B78–B84, May 2010.

[16] J. D. Rolston, "A low-cost multielectrode system for data acquisition enabling real-time closed-loop processing with rapid recovery from stimulation artifacts," *Frontiers Neuroeng.*, vol. 2, p. 12, Jul. 2009.

[17] D. A. Schwarz *et al.*, "Chronic, wireless recordings of large-scale brain activity in freely moving rhesus monkeys," *Nature Methods*, vol. 11, no. 6, p. 670, 2014.

[18] X. Liu, M. Zhang, B. Subei, A. G. Richardson, T. H. Lucas, and J. V. D. Spiegel, "The PennBMBI: Design of a general purpose wireless brain-machine-brain interface system," *IEEE Trans. Biomed. Circuits Syst.*, vol. 9, no. 2, pp. 248–258, Apr. 2015.

[19] C. Mestais, G. Charvet, F. Sauter-Starace, M. Foerster, D. Ratel, and A. L. Benabid, "WIMAGINE: Wireless 64-channel ECoG recording implant for long term clinical applications," *IEEE Trans. Neural Syst. Rehabil. Eng.*, vol. 23, no. 1, pp. 10–21, Jan. 2015.

[20] M. Azin, D. J. Guggenmos, S. Barbay, R. J. Nudo, and P. Mohseni, "A miniaturized system for spike-triggered intracortical microstimulation in an ambulatory rat," *IEEE Trans. Biomed. Eng.*, vol. 58, no. 9, pp. 2589–2597, Sep. 2011.

[21] D. A. Borton, M. Yin, J. Aceros, and A. Nurmikko, "An implantable wireless neural interface for recording cortical circuit dynamics in moving primates," *J. Neural Eng.*, vol. 10, no. 2, Apr. 2013, Art. no. 026010.

[22] R. Muller *et al.*, "A minimally invasive 64-channel wireless μECoG implant," *IEEE J. Solid-State Circuits*, vol. 50, no. 1, pp. 344–359, Jan. 2015.

[23] H. Ando, K. Takizawa, T. Yoshida, K. Matsushita, M. Hirata, and T. Suzuki, "Wireless multichannel neural recording with a 128-mbps UWB transmitter for an implantable brain-machine interfaces," *IEEE Trans. Biomed. Circuits Syst.*, vol. 10, no. 6, pp. 1068–1078, Dec. 2016.

[24] Y. Su, S. Routhu, K. Moon, S. Lee, W. Youm, and Y. Ozturk, "A wireless 32-channel implantable bidirectional brain machine interface," *Sensors*, vol. 16, no. 10, p. 1582, Sep. 2016.

[25] K. Teng, T. Wu, X. Liu, Z. Yang, and C. Heng, "A 400 MHz wireless neural signal processing IC with 625 × on-chip data reduction and reconfigurable BFSK/QPSK transmitter based on sequential injection locking," *IEEE Trans. Biomed. Circuits Syst.*, vol. 11, no. 3, pp. 547–557, Jun. 2017.

[26] J. Xu *et al.*, "A low-noise, wireless, frequency-shaping neural recorder," *IEEE J. Emerg. Sel. Topics Circuits Syst.*, vol. 8, no. 2, pp. 187–200, Jun. 2018.

[27] K. Matsushita *et al.*, "A fully implantable wireless ECoG 128-channel recording device for human brain–machine interfaces: W-HERBS," *Frontiers Neurosci.*, vol. 12, p. 511, Jul. 2018.

[28] Z. He *et al.*, "A wireless powered implantable and flexible neural recording and stimulating system based on NFC protocol," in *Proc. IEEE Int. Conf. Integr. Circuits, Technol. Appl. (ICTA)*, Nov. 2018, pp. 100–101.

[29] P. Yeon, M. S. Bakir, and M. Ghovanloo, "Towards a 1.1 mm^2 free-floating wireless implantable neural recording SoC," in *Proc. IEEE Custom Integr. Circuits Conf. (CICC)*, Apr. 2018, pp. 1–4.

[30] A. Zhou *et al.*, "A wireless and artefact-free 128-channel neuromodulation device for closed-loop stimulation and recording in non-human primates," *Nature Biomed. Eng.*, vol. 3, no. 1, pp. 15–26, 2019.

[31] N. Ahmadi *et al.*, "Towards a distributed, chronically-implantable neural interface," in *Proc. 9th Int. IEEE/EMBS Conf. Neural Eng. (NER)*, Mar. 2019, pp. 719–724.

[32] J. Lee *et al.*, "Neural recording and stimulation using wireless networks of microimplants," *Nature Electron.*, vol. 4, no. 8, pp. 604–614, Aug. 2021.

[33] D. Seo *et al.*, "Wireless recording in the peripheral nervous system with ultrasonic neural dust," *Neuron*, vol. 91, no. 3, pp. 529–539, Apr. 2016.

[34] M. Yin *et al.*, "Wireless neurosensor for full-spectrum electrophysiology recordings during free behavior," *Neuron*, vol. 84, no. 6, pp. 1170–1182, Dec. 2014.

[35] D. Schwarz *et al.*, "Chronic, wireless recordings of large-scale brain activity in freely moving rhesus monkeys," *Nature Methods*, vol. 11, no. 6, p. 670, 2014.

[36] J. Rosenthal, A. Sharma, E. Kampianakis, and M. S. Reynolds, "A 25 Mbps, 12.4 pJ/b DQPSK backscatter data uplink for the NeuroDisc brain-computer interface," *IEEE Trans. Biomed. Circuits Syst.*, vol. 13, no. 5, pp. 858–867, Oct. 2019.

[37] J. Rosenthal and M. S. Reynolds, "A 1.0-Mb/s 198-pJ/bit Bluetooth low-energy compatible single sideband backscatter uplink for the NeuroDisc brain–computer interface," *IEEE Trans. Microw. Theory Techn.*, vol. 67, no. 10, pp. 4015–4022, Oct. 2019.

[38] J. D. Rosenthal and M. S. Reynolds, "Hardware-efficient all-digital architectures for OFDM backscatter modulators," *IEEE Trans. Microw. Theory Techn.*, vol. 69, no. 1, pp. 803–811, Jan. 2021.

[39] A. Hennig and G. V. Bögel, "Analysis of power absorption by human tissue in deeply implantable medical sensor transponders," in *Advanced Microwave Circuits and Systems*. Vukovar, Croatia: InTech, 2010.

[40] J. Day, D. Geddis, J. Kim, S. H. Choi, H. Yoon, and K. D. Song, "Review of radio wave for power transmission in medical applications with safety," *Proc. SPIE*, vol. 9434, Apr. 2015, Art. no. 94340T.

[41] D. Andreuccetti, R. Fossi, and C. Petrucci. (1997). *An Internet Resource for the Calculation of the Dielectric Properties of Body Tissues in the Frequency Range 10 Hz–100 GHz*. [Online]. Available: http://niremf.ifac.cnr.it/tissprop/

[42] G. Lazzi, "Thermal effects of bioimplants," *IEEE Eng. Med. Biol. Mag.*, vol. 24, no. 5, pp. 75–81, Sep./Oct. 2005.

[43] M. Grandolfo, "Worldwide standards on exposure to electromagnetic fields: An overview," *Environmentalist*, vol. 29, no. 2, pp. 109–117, Jun. 2009.

[44] K. Ito, C.-H. Lin, and H. Lin, "Evaluation of wearable and implantable antennas with human phantoms," in *Handbook of Antenna Technologies*. Singapore: Springer, 2015.

[45] Federal Communications Commission. (2020). *Human Exposure to Radiofrequency Electromagnetic Fields*. [Online]. Available: https://www.govinfo.gov/content/pkg/FR-2020-04-06/pdf/2020-06966.pdf

[46] G. L. Barbruni, P. M. Ros, D. Demarchi, S. Carrara, and D. Ghezzi, "Miniaturised wireless power transfer systems for neurostimulation: A review," *IEEE Trans. Biomed. Circuits Syst.*, vol. 14, no. 6, pp. 1160–1178, Dec. 2020.

[47] K. Agarwal, R. Jegadeesan, Y. Guo, and N. Thakor, "Wireless power transfer strategies for implantable bioelectronics," *IEEE Rev. Biomed. Eng.*, vol. 10, pp. 136–161, 2017.

[48] N. Even-Chen *et al.*, "Power-saving design opportunities for wireless intracortical brain–computer interfaces," *Nature Biomed. Eng.*, vol. 4, no. 10, pp. 984–996, Oct. 2020.

[49] S. J. Thomas, E. Wheeler, J. Teizer, and M. S. Reynolds, "Quadrature amplitude modulated backscatter in passive and semipassive UHF RFID systems," *IEEE Trans. Microw. Theory Techn.*, vol. 60, no. 4, pp. 1175–1182, Apr. 2012.

[50] J. F. Ensworth and M. S. Reynolds, "Every smart phone is a backscatter reader: Modulated backscatter compatibility with Bluetooth 4.0 low energy (BLE) devices," in *Proc. IEEE Int. Conf. RFID (RFID)*, Apr. 2015, pp. 78–85.

[51] V. Iyer, V. Talla, B. Kellogg, S. Gollakota, and J. Smith, "Inter-technology backscatter: Towards internet connectivity for implanted devices," in *Proc. ACM SIGCOMM Conf.*, Aug. 2016, pp. 356–369.

[52] Espressif Systems. (2020). *ESP8266EX Datasheet*. [Online]. Available: https://www.espressif.com/sites/default/files/documentation/0a-esp8266ex_da%tasheet_en.pdf

[53] Nordic Semiconductor. (2021). *nRF24L01+ Single Chip 2.4GHz Transceiver Preliminary Product Specification V1.0*. [Online]. Available: https://www.sparkfun.com/datasheets/Components/SMD/nRF24L01Pluss_Prel%iminary_Product_Specification_v1_0.pdf

[54] U.-M. Jow, P. McMenamin, M. Kiani, J. R. Manns, and M. Ghovanloo, "EnerCage: A smart experimental arena with scalable architecture for behavioral experiments," *IEEE Trans. Biomed. Eng.*, vol. 61, no. 1, pp. 139–148, Jan. 2014.

[55] B. Lee, M. Kiani, and M. Ghovanloo, "A smart wirelessly powered homecage for long-term high-throughput behavioral experiments," *IEEE Sensors J.*, vol. 15, no. 9, pp. 4905–4916, Sep. 2015.

[56] S. A. Mirbozorgi, Y. Jia, D. Canales, and M. Ghovanloo, "A wirelessly-powered homecage with segmented copper foils and closed-loop power control," *IEEE Trans. Biomed. Circuits Syst.*, vol. 10, no. 5, pp. 979–989, Oct. 2016.

[57] S. A. Mirbozorgi, H. Bahrami, M. Sawan, and B. Gosselin, "A smart cage with uniform wireless power distribution in 3D for enabling long-term experiments with freely moving animals," *IEEE Trans. Biomed. Circuits Syst.*, vol. 10, no. 2, pp. 424–434, Apr. 2016.

[58] E. Maghsoudloo, G. Gagnon-Turcotte, Z. Rezaei, and B. Gosselin, "A smart neuroscience platform with wireless power transmission for simultaneous optogenetics and electrophysiological recording," in *Proc. IEEE Int. Symp. Circuits Syst. (ISCAS)*, May 2018, pp. 1–5.

[59] H. Mei, K. A. Thackston, R. A. Bercich, J. G. R. Jefferys, and P. P. Irazoqui, "Cavity resonator wireless power transfer system for freely moving animal experiments," *IEEE Trans. Biomed. Eng.*, vol. 64, no. 4, pp. 775–785, Apr. 2017.

[60] B. Lee and Y. Jia, "Wirelessly-powered cage designs for supporting long-term experiments on small freely behaving animals in a large experimental arena," *Electronics*, vol. 9, no. 12, p. 1999, Nov. 2020.

[61] S. Sriram, S. Avlani, M. P. Ward, and S. Sen, "Electro-quasistatic animal body communication for untethered rodent biopotential recording," *Sci. Rep.*, vol. 11, no. 1, p. 3307, Feb. 2021.

[62] A. Sharma, E. Kampianakis, J. Rosenthal, A. Pike, A. Dadkhah, and M. S. Reynolds, "Wideband UHF DQPSK backscatter communication in reverberant cavity animal cage environments," *IEEE Trans. Antennas Propag.*, vol. 67, no. 8, pp. 5002–5011, Aug. 2019.

[63] M. Piangerelli *et al.*, "A fully integrated wireless system for intracranial direct cortical stimulation, real-time electrocorticography data transmission, and smart cage for wireless battery recharge," *Frontiers Neurol.*, vol. 5, p. 156, Aug. 2014.

[64] M. P. Powell, W. R. Britz, J. S. Harper, and D. A. Borton, "An engineered home environment for untethered data telemetry from nonhuman primates," *J. Neurosci. Methods*, vol. 288, pp. 72–81, Aug. 2017.

[65] J. D. Rosenthal, A. Pike, S. Reyes, and M. S. Reynolds, "Electronic mode stirring for improved backscatter communication link margin in a reverberant cavity animal cage environment," *IEEE Trans. Antennas Propag.*, early access, Aug. 9, 2021, doi: 10.1109/TAP2021.3102047.

[66] H. Jiang *et al.*, "A low-frequency versatile wireless power transfer technology for biomedical implants," *IEEE Trans. Biomed. Circuits Syst.*, vol. 7, no. 4, pp. 526–535, Aug. 2013.

[67] X. Liu, M. Zhang, A. G. Richardson, T. H. Lucas, and J. Van der Spiegel, "Design of a closed-loop, bidirectional brain machine interface system with energy efficient neural feature extraction and PID control," *IEEE Trans. Biomed. Circuits Syst.*, vol. 11, no. 4, pp. 729–742, Aug. 2017.

[68] International Telecommunication Union. *ITU Radio Regulations, Chapter II Frequencies, Article 5 Frequency Allocations, Section IV–Table of Frequency Allocations*. Accessed: Oct. 11, 2021. [Online]. Available: https://www.itu.int/pub/R-REG-RR-2020

[69] AirFuel Alliance. (Jun. 2021). *Frequency Choice*. [Online]. Available: https://airfuel.org/frequency-choice/

[70] D. M. Pozar, *Microwave Engineering*, 4th ed. Hoboken, NJ, USA: Wiley, 2012.

[71] C. A. Chestek *et al.*, "HermesC: Low-power wireless neural recording system for freely moving primates," *IEEE Trans. Neural Syst. Rehabil. Eng.*, vol. 17, no. 4, pp. 330–338, Aug. 2009.

[72] Intan Technologies, LLC. *RHS2000 Series Digital Stimulator and Amplifier Chips*. [Online]. Available: http://intantech.com/

[73] S. Zanos, I. Rembado, D. Chen, and E. E. Fetz, "Phase-locked stimulation during cortical beta oscillations produces bidirectional synaptic plasticity in awake monkeys," *Curr. Biol.*, vol. 28, no. 16, pp. 2515–2526, Aug. 2018.

[74] T. G. Petrie, J. Rosenthal, and M. S. Reynolds, "A low-cost 1 Mbps frequency shift keying backscatter receiver and carrier wave generator system for wireless neural recording," in *Proc. IEEE Int. Conf. RFID (RFID)*, Sep. 2020, pp. 1–5.

[75] Multi Channel Systems GmBH. (2021). *Wireless Systems*. [Online]. Available: https://www.multichannelsystems.com/products/wireless-systems

[76] B. H. Waters, A. P. Sample, and J. R. Smith, "Adaptive impedance matching for magnetically coupled resonators," in *Proc. Prog. Electromagn. Res. Symp.*, Moscow, Russia, Aug. 2012, pp. 694–701.

[77] A. Kumar Sharma *et al.*, "Magnetic induction-based non-conventional media communications: A review," *IEEE Sensors J.*, vol. 17, no. 4, pp. 926–940, Dec. 2017.

[78] D. L. Means and K. W. Chan, "Evaluating compliance with FCC guidelines for human exposure to radiofrequency electromagnetic fields," in *Federal Communications Commission Office of Engineering and Technology*. Washington, DC, USA: OET Bulletin, 2001.

[79] A. P. Sample, D. T. Meyer, and J. R. Smith, "Analysis, experimental results, and range adaptation of magnetically coupled resonators for wireless power transfer," *IEEE Trans. Ind. Electron.*, vol. 58, no. 2, pp. 544–554, Feb. 2011.

[80] N. Y. Kim, K. Y. Kim, J. Choi, and C.-W. Kim, "Adaptive frequency with power-level tracking system for efficient magnetic resonance wireless power transfer," *Electron. Lett.*, vol. 48, no. 8, pp. 452–454, Apr. 2012.

[81] Y. Lim, H. Tang, S. Lim, and J. Park, "An adaptive impedance-matching network based on a novel capacitor matrix for wireless power transfer," *IEEE Trans. Power Electron.*, vol. 29, no. 8, pp. 4403–4413, Aug. 2014.

[82] P. D. Wolf, "Indwelling neural implants: Strategies for contending with the *in vivo* environment," in *Thermal Considerations for the Design of an Implanted Cortical Brain—Machine Interface (BMI)*. Boca Raton, FL, USA: CRC Press, 2008, ch. 3.

[83] S. J. Thomas, R. R. Harrison, A. Leonardo, and M. S. Reynolds, "A battery-free multichannel digital neural/EMG telemetry system for flying insects," *IEEE Trans. Biomed. Circuits Syst.*, vol. 6, no. 5, pp. 424–436, Oct. 2012.

[84] S. Naderiparizi, A. N. Parks, Z. Kapetanovic, B. Ransford, and J. R. Smith, "WISPCam: A battery-free RFID camera," in *Proc. IEEE Int. Conf. (RFID)*, Apr. 2015, pp. 166–173.

[85] D. J. Yeager, J. Holleman, R. Prasad, J. R. Smith, and B. P. Otis, "NeuralWISP: A wirelessly powered neural interface with 1-m range," *IEEE Trans. Biomed. Circuits Syst.*, vol. 3, no. 6, pp. 379–387, Dec. 2009.

[86] J. Rosenthal and M. S. Reynolds, "A dual-band shared-hardware 900 MHz 6.25 Mbps DQPSK and 2.4 GHz 1.0 mbps Bluetooth low energy (BLE) backscatter uplink for wireless brain-computer interfaces," in *Proc. IEEE Int. Conf. RFID (RFID)*, Sep. 2020, pp. 1–6.

[87] J. Rosenthal, A. Pike, and M. S. Reynolds, "A 1 Mbps 158 pJ/bit Bluetooth low energy (BLE) compatible backscatter communication uplink for wireless neural recording in an animal cage environment," in *Proc. IEEE Int. Conf. RFID (RFID)*, Apr. 2019, pp. 1–6.

[88] S. Thomas and M. Reynolds, "A 96 Mbit/sec, 15.5 pJ/bit 16-QAM modulator for UHF backscatter communication," in *Proc. IEEE RFID*, Orlando, FL, USA, Apr. 2012, pp. 185–190.

[89] A. Ebrazeh and P. Mohseni, "30 pJ/b, 67 Mbps, centimeter-to-meter range data telemetry with an IR-UWB wireless link," *IEEE Trans. Biomed. Circuits Syst.*, vol. 9, no. 3, pp. 362–369, Jun. 2015.

[90] A. Bertrand *et al.*, "Beamforming approaches for untethered, ultrasonic neural dust motes for cortical recording: A simulation study," in *Proc. 36th Annu. Int. Conf. IEEE Eng. Med. Biol. Soc.*, Aug. 2014, pp. 2625–2628.

[91] A. Dadkhah, J. Rosenthal, and M. S. Reynolds, "ZeroScatter: Zero-added-component backscatter communication using existing digital I/O pins," in *Proc. IEEE Topical Conf. Wireless Sensors Sensor Netw. (WiSNet)*, Jan. 2019, pp. 1–3.

[92] S. J. Thomas, B. P. Degnan, C. Callupe Chavez, and B. Culver, "Backscatter ex-nihilo: Single-component, fully-passive backscattering for microcontrollers," in *Proc. IEEE Int. Conf. RFID (RFID)*, Sep. 2020, pp. 1–6.

[93] S. J. Thomas and J. A. Howe, "Achieving multistate vector scattering with unmodified digital input/output pins," *IEEE J. Radio Freq. Identificat.*, vol. 5, no. 3, pp. 311–316, Sep. 2021.

[94] D. Kim, M. A. Ingram, and W. W. Smith, "Measurements of small-scale fading and path loss for long range RF tags," *IEEE Trans. Antennas Propag.*, vol. 51, no. 8, pp. 1740–1749, Aug. 2003.

[95] J. D. Griffin and G. D. Durgin, "Complete link budgets for backscatter-radio and RFID systems," *IEEE Antennas Propag. Mag.*, vol. 51, no. 2, pp. 11–25, Apr. 2009.

[96] J. Rosenthal and M. S. Reynolds, "A 158 pJ/bit 1.0 Mbps Bluetooth low energy (BLE) compatible backscatter communication system for wireless sensing," in *Proc. IEEE Top. Conf. Wireless Sensors Sensor Netw. (WiSNet)*, Jan. 2019, pp. 1–3.

[97] (May 2021). *Wibotic Hardware*. [Online]. Available: https://www.wibotic.com/products/hardware/

[98] A. Sharma, "Dual-band power and communication antennas for wireless brain-computer interfaces," Ph.D. dissertation, Dept. EE, Univ. Washington, Seattle, WA, USA, 2019.

[99] *Modular Primate Cage Units: Lab Animal Housing & Equipment*. Accessed: Oct. 11, 2021. [Online]. Available: https://labproductsinc.com/product/modular-primate-cage-units/

[100] J. Rosenthal and M. S. Reynolds, "All-digital single sideband (SSB) Bluetooth low energy (BLE) backscatter with an inductor-free, digitally-tuned capacitance modulator," in *IEEE MTT-S Int. Microw. Symp. Dig.*, Aug. 2020, pp. 468–471.

[101] E. Kampianakis, "High data-rate ultra low-power backscatter wireless communication systems for brain-computer interfaces," Ph.D. dissertation, Dept. EE, Univ. Washington, Seattle, WA, USA, 2019.

[102] J. F. Ensworth, "Ultra-low-power Bluetooth low energy (BLE) compatible backscatter communication and energy harvesting for battery-free wearable devices," Ph.D. dissertation, Dept. EE, Univ. Washington, Seattle, WA, USA, Dec. 2016.

[103] J. F. Ensworth, A. T. Hoang, T. Q. Phu, and M. S. Reynolds, "Full-duplex Bluetooth low energy (BLE) compatible backscatter communication system for mobile devices," in *Proc. IEEE Top. Conf. Wireless Sensors Sensor Netw. (WiSNet)*, Phoenix, AZ, USA, Jan. 2017, pp. 45–48.

[104] B. Lee *et al.*, "An inductively-powered wireless neural recording and stimulation system for freely-behaving animals," *IEEE Trans. Biomed. Circuits Syst.*, vol. 13, no. 2, pp. 413–424, Apr. 2019.

[105] X. Shi and J. R. Smith, "Reconfigurable and adaptive coupled relay resonator platform for a moving receiver," in *Proc. Int. Workshop Antenna Technol. (iWAT)*, Mar. 2019, pp. 182–185.

ABOUT THE AUTHORS

Gregory E. Moore (Member, IEEE) received the B.S. degree in physics and the B.S. degree in electrical engineering from the University of Maryland, College Park, MD, USA, in 2005, and the M.S. degree in electrical engineering from the University of Washington, Seattle, WA, USA, in 2018.

From 2008 to 2012, he was an Electrical Engineer with Tao of Systems Integration, Inc., Hampton, VA, USA, where he was engaged in mixed-signal circuit and control systems' design for flow measurement products for aeronautics/marine engineering. He is currently a Research Assistant with the University of Washington. His research involves WPT and low-power communication design, with a special focus on applications directed toward biopotential stimulation, recording, and telemetry.

James D. Rosenthal (Member, IEEE) received the B.S. degree in electrical engineering from the University of Minnesota, Minneapolis, MN, USA, in 2013, and the M.S. and Ph.D. degrees in electrical engineering from the University of Washington, Seattle, WA, USA, in 2018 and 2021, respectively.

From 2013 to 2016, he was an Electrical Engineer with the NASA Langley Research Center, Hampton, VA, USA, where he designed avionics systems for aerospace research. From 2016 to 2021, he was a Research Assistant and an NSF Graduate Research Fellow with the Department of Electrical and Computer Engineering, University of Washington. He is currently a Marie Skłodowska-Curie Postdoctoral Research Fellow with the Swiss Federal Institute of Technology Lausanne (EPFL), Lausanne, Switzerland. His research focuses on the design of ultralow-power backscatter communication systems for bioelectronic medical devices.

Joshua R. Smith (Fellow, IEEE) received the B.A. degree in computer science and philosophy from Williams College, Williamstown, MA, USA, in 1991, the M.A. degree in physics from the University of Cambridge, Cambridge, U.K., in 1997, and the S.M. and Ph.D. degrees from the Massachusetts Institute of Technology, Cambridge, MA, USA, in 1995 and 1999, respectively.

Before joining the University of Washington, Seattle, WA, USA, he was a Principal Engineer with Intel Corporation, Seattle. He is a Co-Founder of three companies that are commercializing research from his lab: Wibotic, Seattle, is applying near field resonant WPT for applications, such as recharging robots and powering implanted devices; Jeeva Wireless, Seattle, makes low power backscatter communication products; and Proprio, Seattle, provides surgical visualization and navigation technology. He is currently the Milton and Delia Zeutschel Professor, jointly appointed in the Allen School of Computer Science and Engineering and the Department of Electrical and Computer Engineering, with the University of Washington.

Matthew S. Reynolds (Senior Member, IEEE) received the S.B., M.Eng., and Ph.D. degrees from the Massachusetts Institute of Technology (MIT), Cambridge, MA, USA, in 1998, 1999, and 2003, respectively.

He is currently an Associate Professor of electrical and computer engineering with the University of Washington, Seattle, WA, USA. He is a Co-Founder of the RFID systems firm, ThingMagic Inc., Sunnyvale, CA, USA; the demand-side energy conservation technology firm Zensi; the home sensing company SNUPI Inc., Seattle; and the millimeter-wave imaging firm ThruWave Inc., Seattle. His research interests include the physics of sensors and actuators, radio frequency identification (RFID), microwave and millimeter-wave imaging, and sensor signal processing.